ACS APPLIED MATERIALS & INTERFACES

www.acsami.org

Research Article

Entrapment and Voltage-Driven Reorganization of Hydrophobic Nanoparticles in Planar Phospholipid Bilayers

Colin M. Basham, Stephanie Spittle, Joshua Sangoro, Joyce El-Beyrouthy, Eric Freeman, and Stephen A. Sarles*

Cite This: *ACS Appl. Mater. Interfaces* 2022, 14, 54558–54571

Read Online

ACCESS | Metrics & More | Article Recommendations | Supporting Information

ABSTRACT: Engineered nanoparticles (NPs) possess diverse physical and chemical properties, which make them attractive agents for targeted cellular interactions within the human body. Once affiliated with the plasma membrane, NPs can become embedded within its hydrophobic core, which can limit the intended therapeutic functionality and affect the associated toxicity. As such, understanding the physical effects of embedded NPs on a plasma membrane is critical to understanding their design and clinical use. Here, we demonstrate that functionalized, hydrophobic gold NPs dissolved in oil can be directly trapped within the hydrophobic interior of a phospholipid membrane assembled using the droplet interface bilayer technique. This approach to model membrane formation preserves lateral lipid diffusion found in cell membranes and permits simultaneous imaging and electrophysiology to study the effects of embedded NPs on the electromechanical properties of the bilayer. We show that trapped NPs enhance ion conductance and lateral membrane tension in 1,2-dioleoyl-*sn*-glycero-3-phosphocholine (DOPC) and 1,2-diphytanoyl-*sn*-glycero-3-phosphocholine (DPhPC) bilayers while lowering the adhesive energy of the joined droplets. Embedded NPs also cause changes in bilayer capacitance and area in response to applied voltage, which are nonmonotonic for DOPC bilayers. This electrophysical characterization can reveal NP entrapment without relying on changes in membrane thickness. By evaluating the energetic components of membrane tension under an applied potential, we demonstrate that these nonmonotonic, voltage-dependent responses are caused by reversible clustering of NPs within the unsaturated DOPC membrane core; aggregates form spontaneously at low voltages and are dispersed by higher transmembrane potentials of magnitude similar to those found in the cellular environment. These findings allow for a better understanding of lipid-dependent NP interactions, while providing a platform to study relationships between other hydrophobic nanomaterials and organic membranes.

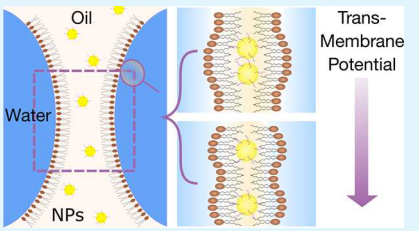

KEYWORDS: *phospholipid bilayer, gold nanoparticles, hydrophobic nanomaterials, electrophysiology, nanoparticle–membrane interactions, electrical pressure, membrane tension*

INTRODUCTION

From both therapeutic and technological perspectives, interest in the interactions between engineered nanomaterials and biological membranes has blossomed in the last decade. Nanoparticles (NPs) have been shown to alter both the structure and physical properties of the membrane.[1] For example, embedded NPs can control liposomal permeability for drug delivery,[2−4] while carbon nanotubes are known to enhance electrical conductivity and transport properties in planar membranes.[5−7] This deliberate combination of material properties, known as inorganics-*in*-organics,[8] often generates unique results; for example, conductive gold NPs embedded in insulative phospholipid membranes can behave as single electron transistors.[9] A further application of membrane–NP integration is in diagnostic cellular imaging, where membrane-affiliated NPs enhance fluorescence and act as contrasting agents within biological membranes.[10−13] This facilitates targeted cellular imaging and even the detection of trans-membrane potentials.[14]

In the context of drug delivery, NPs interact with the plasma membrane en route to delivering their payloads to a cell. Membrane translocation is aided by hydrophobic functionalization of the NP, which helps drive insertion into the hydrophobic membrane interior and also prevents surface fouling in the bloodstream.[15−17] However, this functionalization can also cause hydrophobic NPs to accumulate in the core of the membrane.[16] While gold NPs are desirable delivery agents due to their optical and thermal properties, few treatments involving gold NPs are currently approved by the FDA, due in part to cytotoxic interactions with cellular membranes.[18] Embedded NPs can alter membrane thickness and slow bending fluctuations, which can alter membrane

Received: September 15, 2022
Accepted: November 18, 2022
Published: December 2, 2022

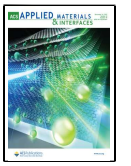

protein function and enzyme catalysis.[19−21] Further, NP loading can affect lipid tail disorder and phase behaviors, influencing biophysical processes such as passive transport and vesicle budding.[21−23] Because many of these effects are observed from computational studies, sensitive experimental methods are needed to validate the effects of candidate NPs interacting with and embedding in a membrane.

Several methods are presently used to entrap NPs in a phospholipid bilayer. Lipid vesicles may be loaded with hydrophobic NPs via extrusion or dialysis,[24−26] a process that can be enhanced by chloroform annealing[27] or assembly with water−oil−water double emulsions.[22] Nonlipid surfactant vesicles have also been used to trap NPs,[10,20] as they can offer enhanced durability over conventional lipids. Vesicles loaded with NPs or quantum dots can then be fused onto supportive substrates to form planar supported lipid bilayers (SLBs) doped with hydrophobic inclusions.[9,28] These methods allow membrane properties such as lipid orientation and membrane fluidity to be probed using microscopic and spectroscopic techniques, and the use of closed vesicles can mimic physical aspects of the cellular environment such as membrane curvature.

However, the strain induced by high curvature of spherical vesicles complicates NP loading,[29] and conventional vesicle assembly offers poor control of embedded NP concentrations, sometimes resulting in Janus-like or bare vesicles.[22,24] This can also cause inconsistent NP loading in SLBs,[9] which complicates the study of doped-membrane properties. Further, the supportive substrates of SLBs can artificially influence lipid phase transitions[30] and interfere with trapped NP distribution by encouraging aggregation or pushing NPs into the exterior lipid leaflet.[9,28] These issues consequently obscure electrophysiology measurements of doped membranes, which are influenced by the amounts and relative locations of trapped NPs[31] and can further reveal potential collective effects of embedded NPs and transmembrane potentials. Such electric fields play vital regulatory roles in cellular behaviors: For example, transmembrane electrical potentials affect cell proliferation, neuronal migration, and the uptake of antibiotic peptides.[32−35] While embedded hydrophobic NPs can lower membrane capacitance,[15,36] the coupled electrical and structural properties of doped lipid membranes (e.g., the relationship between membrane capacitance and thickness) under applied transmembrane potentials remain poorly understood.

In response, we demonstrate a facile, repeatable way of loading hydrophobic NPs into a planar lipid bilayer. This was done using the droplet interface bilayer (DIB) method, which forms a phospholipid membrane between the interface of two lipid-coated aqueous droplets in oil. By dissolving hydrophobic NPs into the oil phase, we show that entrapment can be induced by sandwiching NPs between connecting droplets, which is confirmed by changes in mechanical and electrical properties of the membrane. For the purpose of studying membrane-embedded NPs, this method circumvents several problems of introducing functionalized NPs into the aqueous phase adjacent to the bilayer, including potentially significant energy barriers for bilayer penetration[16] and the tendency of NPs to affect the morphology of assembling lipid monolayers.[37] Further, DIBs provide high electrical resistance and minimal leakage paths, ensuring precision in electrical measurements of membrane structure and transport.[38]

In this work, we leverage electrical measurements and brightfield imaging to quantify the entrapment of hydrophobic NPs in 1,2-dioleoyl-*sn*-glycero-3-phosphocholine (DOPC) and 1,2-diphytanoyl-*sn*-glycero-3-phosphocholine (DPhPC) DIBs assembled in hexadecane or decane oil. Capacitive currents reveal that the solvent-controlled thickness of the membrane determines whether NP entrapment occurs, lipid type influences how NPs are distributed within the membrane, and residual oil is preferentially excluded at high voltages. We discover that DOPC membranes containing embedded hydrophobic NPs exhibit nonmonotonic changes in bilayer area and capacitance with increasing voltage. By quantifying the lateral tension components of NP-doped membranes, we explain how transmembrane voltage reversibly redistributes NPs within the bilayer hydrophobic core in ways that affect measured membrane thickness, tension, and adhesive energy. In contrast, NP distributions trapped within stiffer DPhPC bilayers appear to be less malleable under voltage. These differences demonstrate how both lipid compositions and transmembrane potentials affect NP organization in the hydrophobic membrane interior and thereby illuminate a more complete picture of in vivo particle interactions within the cell membrane.

RESULTS

Characterization of Hydrophobic NPs in Oil. Since gold NPs are introduced to the bilayer via the oil, we first assessed the diameters of ligand-coated NPs solvated in either *n*-decane (C10) or *n*-hexadecane (C16) and measured the corresponding electrical properties of NP−oil solutions. The NPs had a core diameter of 3.3 ± 0.5 nm, as specified by the vendor; this was confirmed with transmission electron microscopy (TEM) images of dispersed NPs (n = 50) in a lipid−NP mixture (Figure S1A). Figure S1A also appears to show single hydrophobic NPs embedded in the vesicle membrane, as has been reported elsewhere,[27] while NP aggregates were observed in the interstitial space surrounding the vesicle. The NPs were functionalized with hydrophobic octanethiol (OT) ligands, which were expected to add ∼0.8 nm to the ∼1 to 2 nm radius of the gold cores.[24,27] Indeed, dynamic light scattering (DLS) measurements revealed that solvated particles had average diameters of 5.9 ± 1.3 and 5.0 ± 1.0 nm in C10 and C16, respectively, consistent with OT ligands extending into the oil. Further information on DLS measurements, including values of polydispersity, is reported in Figure S1, where the presence of dominant intensity peaks below 10 nm confirmed that most of the NPs were well dissolved. The larger diameter of particles in C10 aligned with our observation that NPs solvated more readily in C10 at room temperature, whereas NPs in C16 required mixing overnight to obtain a well-dispersed NP solution. Sonication of NP-oil solutions was found to induce particle aggregation (Figure S1C) and thus was not performed when preparing solutions for bilayer experiments.

To characterize the electrical properties of the NP solutions, we performed impedance spectroscopy on NPs dissolved in C10 and examined the real parts of both the complex dielectric function (Figure S2A) and complex conductivity function (Figure S2B). From Figure S2A, it was determined that the static dielectric permittivity, or dielectric constant (ε), of neat *n*-decane was approximately 1.7 with no significant variation across the 0.1−10^6 Hz frequency range. However, the addition of 0.01 mg/mL NPs resulted in a frequency-dependent permittivity below 10 Hz, as well as an increase in the value

https://doi.org/10.1021/acsami.2c16677
ACS Appl. Mater. Interfaces 2022, 14, 54558−54571

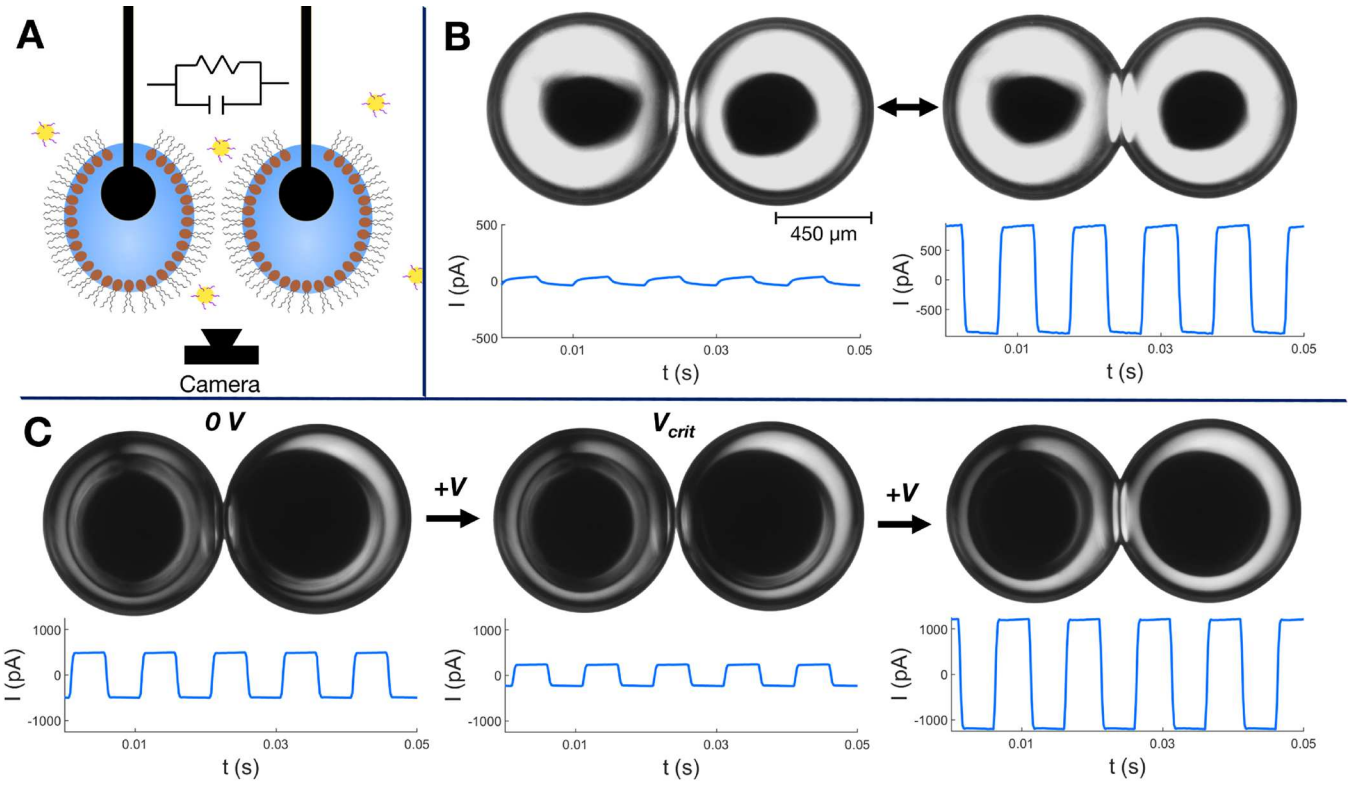

Figure 1. (A) A DIB is formed by connecting two lipid-coated aqueous droplets in an oil phase, which may contain gold NPs. Integrated electrodes and cameras monitor the electrical and mechanical properties. The electrical path across the bilayer is evaluated as a parallel RC circuit. (B) Growth in membrane area and capacitive current (left to right) confirms bilayer formation. This process occurred spontaneously in a neat oil phase but required an initiation voltage when NPs were present. For DPhPC bilayers formed in C10 + NPs, removal of DC voltage causes the membrane to dissociate (left). (C) DOPC bilayers formed in C10 + NPs remain intact upon removal of DC voltage (left). Increasing the DC voltage reduces capacitive current and bilayer area (middle), until exceeding a critical voltage causes the bilayer capacitance and area to grow (right).

of the dielectric constant to ∼1.8 at frequencies above 10 Hz. Increasing the concentration of dissolved NPs to 0.5 mg/mL did not significantly affect the complex dielectric function or change the value of the dielectric constant. The high frequency plateau is likely because the dipoles of the gold NPs do not have time to orient in the direction of the oscillating electric field at higher frequencies;[39] thus, probing the system at frequencies above 10 Hz minimizes the contributions of the permittivity of the gold NP core to the effective permittivity of the mixture. On the other hand, conductivity measurements of the solutions, shown in Figure S2B, revealed that addition of NPs significantly increased solution conductivity by an amount proportional to the concentration of NPs. Together, these results demonstrate that the addition of 0.5 mg/mL or less OT-decorated gold NPs causes only a small increase (∼6%) on the dielectric constant of *n*-decane at frequencies above 10 Hz, despite significant increases in conductivity.

Oil-Solvated NPs Affect Energetics of DIB Formation. To trap hydrophobic NPs within a planar phospholipid membrane, DIBs were formed by bringing into contact pairs of lipid-coated aqueous droplets (each ∼400 nL in volume) in NP−oil solution (Figure 1A). Two separate lipid types were used to form phospholipid membranes: DPhPC and DOPC. DPhPC is of archaeal origin and was selected for its rigidity and membrane stability,[40] while unsaturated DOPC was chosen to yield a fluid, biomimetic membrane. Chemical structures of these phospholipids, in addition to those for the OT ligand and both *n*-alkane oils, are compared in Figure S3. Lipids were incorporated as unilamellar vesicles into the aqueous droplets. Wire-type silver−silver chloride electrodes inserted into the aqueous droplets allowed for mechanical manipulation of the droplets and electrical interrogation of the interfacial bilayer, which is effectively modeled as a parallel RC circuit (Figure 1A).[41] Bilayer formation occurs when excess solvent is entropically excluded from between the opposing lipid monlayers,[42] creating a thinned planar membrane that adheres the droplets. The resulting thickness of the bilayer depends on the size of the oil molecule,[43] where larger oil molecules are excluded more efficiently than smaller oils. Since C10 is smaller than C16, more oil is retained in the membrane upon thinning and, thus, the bilayer has a larger hydrophobic thickness.[44]

Spontaneous bilayer formation was observed after a few minutes when droplets were connected in neat oil (C16 or C10), as indicated by increases in the illuminated contact area and measured capacitive current (Figure 1B, right vs left).[44,45] However, spontaneous bilayer formation was not observed, even 10 min after contact, for any lipid/oil combinations containing at least 0.1 mg/mL NPs in the organic phase. This presumably thicker interface minimized the disjoining pressure between opposing monolayers and required a counterbalancing pressure to spur attractive interactions between the droplets.[46,47] We achieved this by applying DC voltage, which was increased iteratively until thinning occurred, as confirmed via imaging and measurements of capacitive current. The value of the required *initiation voltage* varied with lipid and oil type, and we discovered that higher concentrations of NPs in the oil required higher voltages to induce bilayer formation

https://doi.org/10.1021/acsami.2c16677
ACS Appl. Mater. Interfaces 2022, 14, 54558−54571

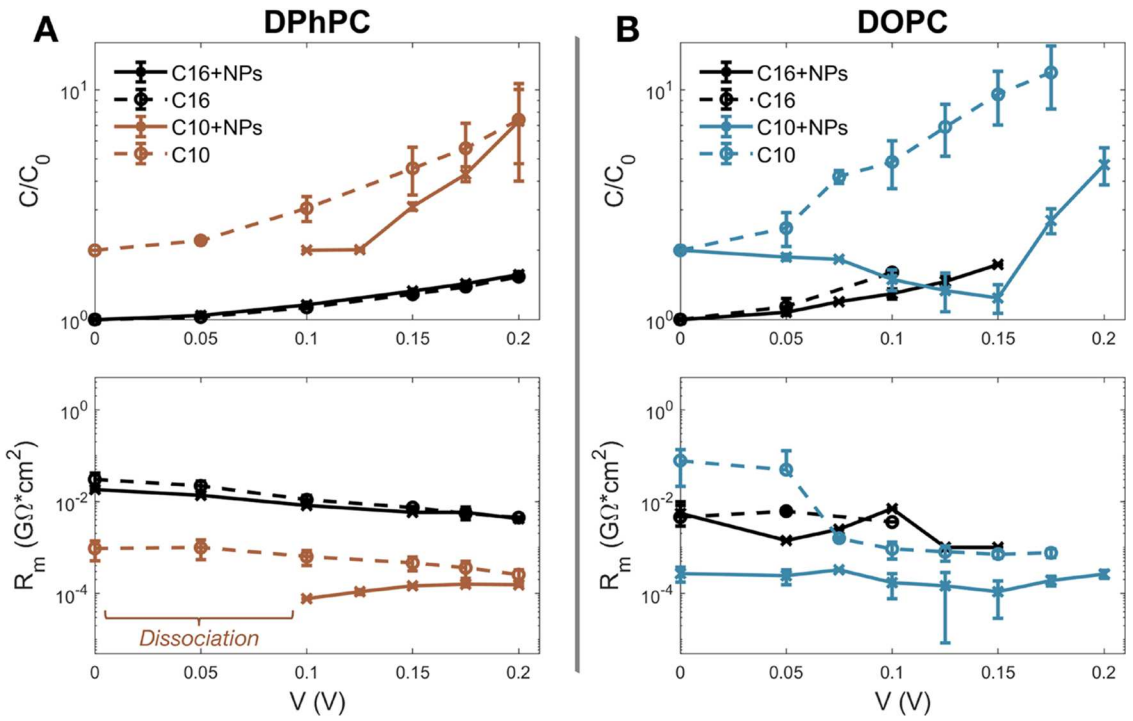

Figure 2. Normalized capacitance (C/C_0) and specific resistance (R_m) with respect to voltage for (A) DPhPC and (B) DOPC DIBs. Data represents DIBs formed in *n*-hexadecane (C16, black) and *n*-decane (C10, colored) with or without hydrophobic NPs. Dotted lines represent control cases with no NPs. Total NP concentration in oil is 0.1 mg/mL. The discretized data points represent the mean of values obtained from multiple bilayers ($2 \leq n \leq 7$), while error bars represent one standard deviation. C/C_0 data for C10 are offset by +1 unit for clarity.

(Table S1). Moreover, droplets generally remained adhered when the applied DC voltage was subsequently reduced to 0 V. The average zero-volt membrane areas are reported in Table S1 and were found to be similar in C16, whether or not NPs were present; however, the presence of NPs slightly increased the zero-volt area of the bilayer when formed in C10. There is one exception: DPhPC-coated droplets connected in C10 + NPs spontaneously dissociated after voltage-induced bilayer thinning at holding potentials below |100 mV|. *Dissociation* is characterized by a complete reduction of contact area and elimination of capacitive current, and it sometimes resulted in droplets visibly drifting apart, as shown in Figure 1B (left). Both the need for an initiation voltage and the observation that droplets could self-separate at biases below this threshold demonstrated that dissolved hydrophobic NPs alter the energetics of droplet adhesion.

Voltage-Dependent Properties Reveal that Bilayers Entrap NPs in C10, Not C16. To determine whether hydrophobic NPs were indeed trapped in the membrane upon bilayer formation, we probed the electrical capacitance, *C*, and resistance, *R*, by measuring the current induced by a low-amplitude triangular AC voltage (at 100 Hz, where ε is constant) superimposed onto a quasi-static DC voltage (see Methods for more details). This composite signal allowed for assessing quasi-static values of *R* and *C* at different trans-membrane potentials without generating frequency-dependent electrical fields at the gold interface from localized surface plasmon resonance (a MHz phenomenon[48]). Hence, it was possible to determine how these membrane properties change in the presence of NPs. Phospholipid bilayers are subject to thinning and areal expansion in the presence of DC voltage, due to electrocompression and electrowetting effects.[47] These effects contribute to monotonic increases in bilayer capacitance with increasing voltage, as governed by the following equation

$$C(V) = \frac{\varepsilon_0 \varepsilon A(V)}{d(V)} \quad (1)$$

where *C* and *A* are the nominal capacitance and area of the membrane, respectively, ε_0 is the dielectric permittivity of vacuum, ε is the relative permittivity of the dielectric, and *d* is the hydrophobic thickness of the membrane. Thicker bilayers formed in C10 are known to compress more in response to applied voltage as residual oil is excluded from the membrane,[49,50] yielding steeper *C* vs *V* relationships as compared to lipid bilayers formed in C16. We hypothesized that trapped particles would affect this relationship, along with the electrical resistance of the bilayer.

Figure 2 shows bilayer capacitance normalized by its zero-volt value (C/C_0) and specific resistance ($R_m = R \times A$) plotted vs the applied DC bias for DIBs formed in the presence and absence of NPs. These data show that C/C_0 vs *V* relations for both DOPC and DPhPC bilayers in the presence of C16 + 0.1 mg/mL NPs were indistinguishable from their respective control cases (C16, no NPs). There were also little differences in the values of R_m for DOPC and DPhPC DIBs in C16 with and without NPs; both lipid types possessed values of specific resistance of ~10 MΩ cm^2 at 0 V, which decreased slightly with increasing voltage. The nominal values of R_m certify that DIBs formed in C16 are highly insulating membranes and suggest that NPs do not significantly disrupt the bilayer to allow for voltage-induced ion transport at a NP concentration of 0.1 mg/mL. In fact, the similarities in both C/C_0 vs V and R_m vs V observed for DPhPC and DOPC DIBs formed in C16 suggest that NPs are mostly excluded from between the lipid leaflets during bilayer formation and few, if any, remain in the

https://doi.org/10.1021/acsami.2c16677
ACS Appl. Mater. Interfaces 2022, 14, 54558−54571

membrane after thinning. This finding makes sense given the characteristic lengths of the NPs and bilayers; most spherical NPs only embed in lipid membranes with hydrophobic thicknesses equal to or greater than their own diameters.[16,27,51−53] Here, using capacitance and area measurements to calculate average bilayer thickness (see eq 2), we found that DOPC and DPhPC DIBs formed in C16 have measured hydrophobic thicknesses of 3.1 ± 0.1 nm at 0 V, in agreement with prior studies.[40] By comparing this value with reported solvent-free DPhPC and DOPC membranes,[50,54] we calculate that these membranes contained approximately 13% oil by volume. This thickness is smaller even than the core diameter of the functionalized NPs, and the size exclusion is likely made stronger by the solvation of OT ligands on the NPs. Measurements reported in Table S1 show that average membrane thickness at 0 V remained unchanged when bilayers were formed in C16 + 0.1 mg/mL NPs, further evidence that few, if any, NPs are entrapped.

Comparatively, DPhPC and DOPC DIBs formed in C10 had mean hydrophobic thicknesses of 4.6 and 5.1 nm, respectively, at 0 V, correlating to 41 and 47% oil by volume (Table S1). In contrast to results discussed above for C16, significant changes to R_m and C/C_0 vs V were observed when DIBs were formed in C10 + 0.1 mg/mL NPs. As represented by Figures 1B and 2A, DPhPC monolayers fully dissociated at voltages below |100| mV. Even when these bilayers were intact at higher potentials, R_m was almost an order of magnitude lower compared to control DPhPC membranes in C10. Larger differences and other behaviors were observed when DOPC DIBs were formed in the presence of NPs. Unlike DPhPC+NP membranes, DOPC+NP membranes remained intact when the DC initiation voltage was removed (Figure 2B). Specific resistance was 10^2−10^3 MΩ cm^2 lower at voltages ≤50 mV when NPs were present. This decrease is not explained by a parallel conductance path around the bilayer (i.e., across the monolayers and through the oil), since values of R_m for DIBs in C16 with and without NPs were nearly identical. Rather, the phospholipid membrane remains the dominant impedance element in the equivalent circuit even when the oil is sufficiently conductive. The data therefore suggest that changes in R_m are caused by NPs in the membrane; for example, an increase in ion conductivity could rise from membrane disruption[23,31] and higher electrical conductivity of entrapped NPs.

Surprisingly, and in contrast to the monotonic increases in C/C_0 vs V due to electrowetting/compression in DPhPC+NP bilayers shown in Figure 2A, we discovered that increasing the applied DC voltage from 0 mV *reduced* the normalized capacitance of DOPC+NP bilayers in C10 (Figures 1C and 2B) until these values reached a minimum at a critical voltage, V_{crit}, which was near 150 mV for a NP concentration of 0.1 mg/mL. Normalized area measurements (A/A_0) are reported in Figure S4 and mirror this trend. At the critical voltage, mean normalized capacitance was 76% lower than its zero-volt value, while mean normalized area decreased by 70%. Only at applied potentials exceeding V_{crit} did C and A increase monotonically with voltage. These trend continued until the membrane ruptured, typically at potentials between 200 and 300 mV. Since a $V_{crit} > 0$ mV was not observed for DPhPC membranes formed in C10, and both lipid types have the same PC headgroup, it is clear that this behavior was influenced by the unsaturated DOPC tails. Thus, while NPs appeared to be excluded from both DOPC and DPhPC DIBs formed in C16, the substantial differences in electrical capacitance and resistance vs voltage measured for DPhPC and DOPC DIBs in C10 indicate association of NPs with the membrane after bilayer thinning. We therefore focus solely on DIBs formed in C10 throughout the rest of this work. Moreover, since the hydrophobic NPs originate from the oil phase in these experiments, we interpret that NPs are retained within the hydrophobic interior of the membrane.

Trapped NPs Induce Concentration-Dependent Structural Changes in DOPC Bilayers. To further explore the influence of entrapped NPs in DOPC bilayers, and to understand their behaviors within the membrane, we studied the electrophysical responses as a function of NP concentration. Figure 3 shows the steady-state responses of nominal

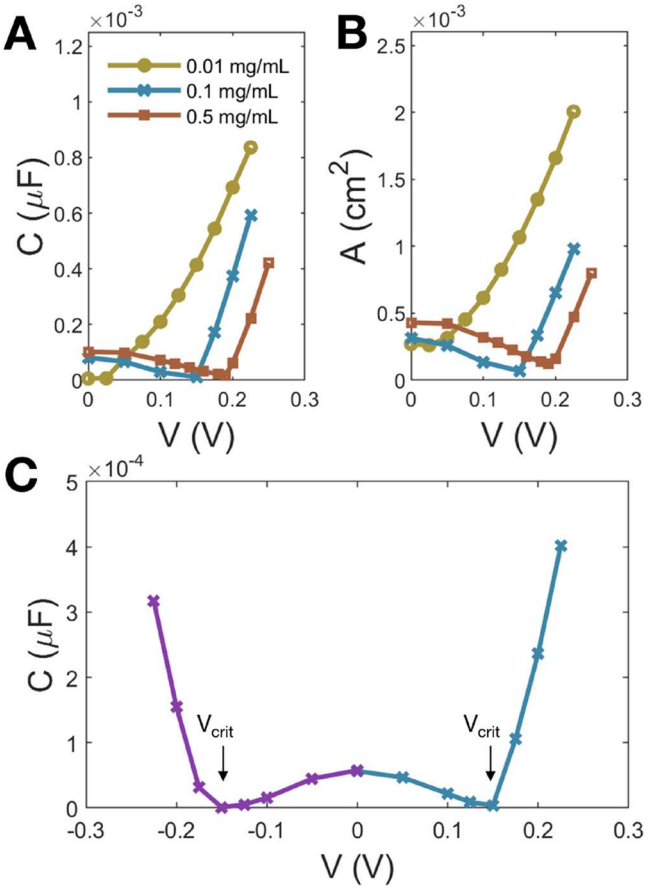

Figure 3. (A) Nominal capacitance, and (B) area, of a DOPC bilayer in C10 as a function of applied voltage, for different NP concentrations: 0.01 mg/mL (yellow), 0.1 mg/mL (blue), and 0.5 mg/mL (orange). (C) Nominal capacitive response of a DOPC bilayer in C10 with 0.1 mg/mL NP concentration at both positive and negative DC voltages.

bilayer capacitance (Figure 3A) and area (Figure 3B, computed assuming a circular interface) vs transmembrane voltage for three concentrations of NPs in C10. At NP concentrations of 0.01 mg/mL, an initiation voltage of ∼130 mV was required for bilayer formation. After formation, the membrane behaved similar to the DOPC in C10 control case (no NPs) in Figure 2B, which displayed quadratic dependences on applied voltage for C and A. At a NP concentration of 0.1 mg/mL, where the initiation voltage was ∼270 mV, both C and A exhibited minimum values at $V_{crit} \approx 150$ mV, before

https://doi.org/10.1021/acsami.2c16677
ACS Appl. Mater. Interfaces 2022, 14, 54558−54571

sharply increasing at higher voltages. At the highest NP concentration tested (0.5 mg/mL), which required more than 300 mV to initiate bilayer formation, V_{crit} increased to ~200 mV. We further observed that the initial membrane area at 0 V increased proportionally with the concentration of NPs in the system (Table S1). While the reason for this relationship is unclear, it has been reported that lipid tail ordering can change in the presence of large or hydrophobic embedded NPs;[55,56] this could change the energetics of membrane adhesion and increase the bilayer area. Due to the dependence of area and capacitance on dissolved NP concentrations and the fact that these droplets never dissociated after their initial voltage-induced formation, it appeared that the amount of NPs in the oil affected the amount trapped in the membrane and its subsequent response to applied potentials.

The number of trapped NPs could affect the conductance of the membrane, as impedance spectroscopy measurements showed that the conductivity of the organic phase depends on the dissolved NP concentration. To examine this, we evaluated DOPC bilayer conductance, normalized by membrane area, vs voltage for various concentrations of NPs. The results are plotted in Figure S5. As expected, the specific conductance (G_s) of the NP-free membrane was much lower at low voltages than for DOPC bilayers containing even the lowest concentration of NPs, though G_s increased with voltage as electrocompression caused the membrane to thin. Interestingly, all three bulk concentrations of NPs induced similar levels of zero-volt conductance within the bilayer (~2 to 4 × 10^{-6} S/cm^2). Thus, while Figure 3 shows a concentration dependence of membrane mechanical properties in response to voltage, it appears that membrane conductance is far less sensitive to the number of trapped NPs. For the higher concentrations of trapped NPs (0.1 and 0.5 mg/mL), G_s peaked at associated V_{crit} values, corresponding to maximum membrane disorder and ion permeability at these voltages.

Minimum capacitance at a nonzero voltage is similar to behavior seen with asymmetrically charged membranes, such as when opposing lipid leaflets possess different dipole potentials. In such a case, an applied voltage adds to the intrinsic membrane potential, resulting in a minimum capacitance at a single potential with equal magnitude and opposite polarity to the intrinsic potential.[57] To see if the entrapped NPs affected the inherent membrane potential which resulted in similar changes of C vs V, we evaluated the capacitance of DOPC + NP membranes in response to both positive and negative applied voltages. Figure 3C shows that, unlike asymmetrically charged lipid membranes which exhibit a single local minimum, capacitance displays local minima at both positive and negative applied voltages. Further, the value of V_{crit} was nearly identical at both polarities. These measurements confirm that V_{crit} originates from NPs trapped within the bilayer, and the applied electric field imposes structural changes on both the NPs and phospholipid bilayer, which are reflected by changes in C and A.

Reversible Changes in Membrane Thickness Reveal NP Retention at High Voltages. Given the steep increases in C and A at voltages above V_{crit} (Figure 3), we questioned whether high transmembrane potentials exclude or retain NPs trapped in DOPC DIBs formed in C10. To test this, we evaluated bilayer thickness across the tested voltage range by measuring the specific capacitance, C_m

$$C_m = \frac{\partial C}{\partial A} = \frac{\varepsilon_0 \varepsilon}{d} \quad (2)$$

which is found by linear regression of C vs A data obtained at multiple bilayer areas controlled by manipulating the electrode positions.[44,50] Hydrophobic thickness, d, was computed using ε = 2.2 (see Methods); repeating this measurement at each DC voltage allowed for understanding how both voltage and NPs affect membrane thickness. Measurements were taken during both increases and decreases in voltage to discern the reversibility of the responses.

Figure 4 shows representative traces for computed hydrophobic thicknesses for DPhPC and DOPC bilayers in C10 in the presence and absence of 0.1 mg/mL NPs. Corresponding C_m measurements are plotted in Figure S6. Pure DPhPC and DOPC DIBs at 0 V yield C_m = 0.422 ± 0.096 and 0.385 ± 0.045 μF/cm^2 ($n \geq 3$), respectively, which lies within the range of reported values for these lipid types when formed in n-decane.[47,50] These values correspond to zero-volt hydrophobic thicknesses of around 5 nm. Interestingly, DPhPC membranes formed in C10 with NPs were of similar thickness to NP-free membranes (Figure 4A). Bilayer thickness decreased with increasing voltage in both cases, caused by the removal of oil from the hydrophobic core of the bilayer due to the applied electric field. For example, core thickness of DPhPC DIBs without NPs decreased from 5.3 nm at 0 V to 3.6 nm at 200 mV, and the retained oil fell from 49 to 24% by volume.

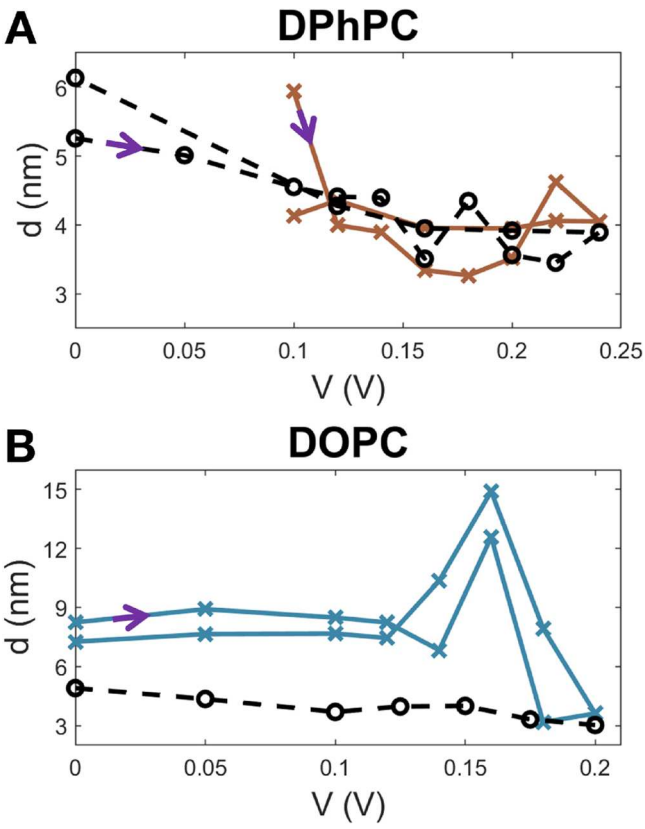

Figure 4. Representative hydrophobic thicknesses of (A) DPhPC and (B) DOPC bilayers in C10, as a function of DC voltage. The dotted black traces represent DIBs formed without NPs, while solid colored traces represent DIBs formed in the presence of NPs at a concentration of 0.1 mg/mL. Purple arrows denote the directions of stepwise voltage measurements.

https://doi.org/10.1021/acsami.2c16677
ACS Appl. Mater. Interfaces 2022, 14, 54558−54571

Likewise, core thickness of DOPC DIBs without NPs decreased from 4.9 nm at 0 V to 3.0 nm at 200 mV, and the volume percentage of oil reduced from 45 to 11%. This thinning response was reversible for increasing and decreasing voltage steps; however, DPhPC + NP bilayers dissociated below 100 mV, while DPhPC bilayers without NPs remained intact at 0 V.

Separately, DOPC + NP membranes were much thicker than regular DOPC bilayers at 0 V, with a mean calculated zero-volt thickness of 7.2 nm. While DOPC membrane thickness decreased slightly with increasing voltage, similar to DPhPC, the DOPC + NP thickness remained constant with increasing voltage and then *increased* greatly at a voltage coinciding with V_{crit}= 160 mV (Figure 4B). This is consistent with the prior observation that normalized capacitance decreased more than normalized area at voltages near V_{crit}, implying a thickening of the hydrophobic section of the membrane. Once V_{crit} was exceeded, thickness decreased until reaching ∼4 nm, matching both the hydrophobic thickness of the control DOPC bilayer and the diameter of the NP cores. When voltage was quasi-statically lowered to 0 V, a similar nonlinear voltage-dependent change in thickness was observed. While it is possible that some entrapped particles were excluded from between the leaflets and ejected into the surrounding oil, the reversible changes in thickness indicated that at least a significant fraction of trapped NPs were retained in the DOPC bilayer throughout the range of tested voltages, consistent with recent MD simulations on membrane-embedded 4 nm OT-functionalized gold NPs under the influence an external electric field.[58] In contrast, changes in thickness were expected to be highly hysteretic if particles were mostly excluded from the membrane under high potentials.

To further explore the possibility that NPs are excluded into the surrounding oil at high voltages, and then spontaneously partition back into the bilayer once the voltage is reduced, we formed a DOPC DIB in neat C10 (without NPs) and performed a stepwise voltage measurement to evaluate capacitance and area changes, similar to that shown in Figures 2 and S4. We then added concentrated NPs in C10 to the bulk oil phase, for a final dissolved concentration of 0.125 mg/mL NPs, while holding the membrane at 50 mV to avoid droplet separation from fluid flow. Then we performed C and A measurements both (1) immediately after and (2) 30 min following NP injection. Finally, we separated the droplets and then reconnected them to form a new DIB in the now-NP-doped oil and performed another stepwise voltage measurement. Figure S7 shows that C and A vs V responses were identical to those of the original DOPC membrane even after an incubation period of 30 min following NP injection. However, the DOPC DIB newly formed in C10 + NPs required the application of an initiation DC voltage for formation and exhibited nonlinear voltage-dependent properties characteristic of NP entrapment. This confirmed that a detectable number of NPs could not spontaneously partition into the hydrophobic core of the bilayer from the oil phase, and, therefore, that the reversibility in bilayer thickness observed for DIBs formed in C10 + NPs was a consequence of NPs being retained in the membrane across all voltages tested.

Estimating the Number of Trapped NPs from Capacitance Measurements. The large differences in average thickness for DOPC DIBs with or without NPs in C10, as reported in Table S1 and Figure 4B, suggest that many NPs are trapped within the hydrophobic membrane core. Estimating the number of NPs and their average center-to-center distance within the membrane can offer better insight on membrane mechanics such as bending energy and particle aggregation.[59] An upper limit to the number of trapped NPs in a DOPC in C10 bilayer is found by assuming that each NP occupies a square space in a two-dimensional lattice within the center of the membrane. Dividing the total membrane area (A_T) by the area per NP (A_{NP}) yields the maximum number of laterally packed NPs. Using a typical value of $A_T = 4.24 \times 10^{-4}$ cm^2 from experiments in Figure 4B, and A_{NP} = (5.9 nm)^2 = 34.81 nm^2 from the solvated diameter of NPs in C10 (Figure S1), we calculate that a maximum of ∼1.2×10^9 NPs could fit laterally within the membrane.

Alternatively, we use the computed thickness values obtained on DOPC DIBs in C10 + NPs to approximate the number of trapped particles needed to increase the average membrane thickness at 0 V. This is done by modeling the membrane as two parallel capacitors of different areas, C_A and C_B, being regions free of NPs or doped with NPs, respectively. C_B is defined as the equivalent capacitance of the two outer lipid monolayers encompassing an inner layer of NPs in *n*-decane. These two capacitors occupy unknown area fractions, A_A and A_B, of A_T. The measurements in Figure 4B and values from impedance spectroscopy and DLS measurements are used in conjunction with eq 1 to solve for the membrane area containing NPs, A_B. Details of these calculations and a schematic of the equivalent capacitance model are found in Figure S8, and the parameters for these calculations are reported in Table S2. By assuming that trapped NPs contribute an additional 5.9 nm to the total hydrophobic thickness of the membrane, we estimate that NPs occupy approximately 77% of the bilayer area. This area fraction corresponds to ∼9.4×10^8 NPs trapped in the bilayer, with an equivalent center-to-center distance of 6.7 nm between particles.

The Supporting Information also provides calculations for the molecular weight of this OT-functionalized NP, discusses assumptions within the model, and considers the number of trapped NPs based upon their concentration and distribution in the bulk oil phase. This value is lower (∼1.6×10^6 NPs) for a dissolved concentration of 0.1 mg/mL NPs and thus provides a theoretical range for the total amount of trapped particles. While this range spans several orders of magnitude, it is likely that the trapped NPs occupy a substantial portion of the total membrane area, since there is a significant difference in the average DOPC membrane thickness with and without NPs. On the other hand, the similar values of DPhPC membrane thicknesses with and without NPs imply that fewer NPs are embedded in the membrane. The high repeatability and accuracy of C_m measurements verify that similar amounts of NPs are trapped in DIBs between experiments.

Trapped NPs Impede Membrane Adhesion and Raise Tension. With evidence to suggest that NPs are both trapped and retained in C10 DIBs, we measured the bilayer tension vs voltage and compared these responses to those obtained with NP-free membranes. Bilayer tension is an indicator of molecular order within the bilayer;[47] higher tension signifies unfavorable molecular interactions, including a larger area per lipid molecule. The apparent bilayer tension, γ_{app}, was evaluated for DPhPC and DOPC membranes in the presence of 0.1 mg/mL NPs. This was done by using Young's Equation[44]

https://doi.org/10.1021/acsami.2c16677
ACS Appl. Mater. Interfaces 2022, 14, 54558−54571

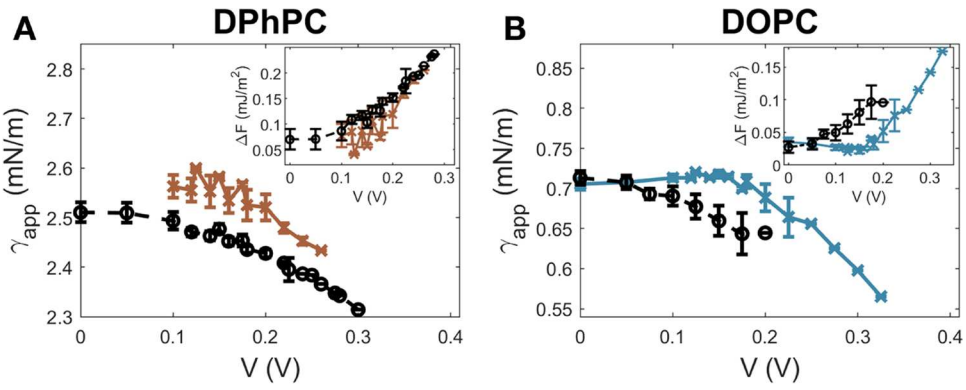

Figure 5. Mean values of apparent bilayer tension of (A) DPhPC and (B) DOPC bilayers in C10 as a function of voltage, $n \geq 5$ for all trials. The dotted black traces represent DIBs formed without NPs, while the solid colored traces represent DIBs with trapped NPs, at a concentration of 0.1 mg/mL. Error bars denote values within one standard deviation. Insets show the energy of adhesion, ΔF, as a function of voltage.

$$\gamma_{app} = 2\gamma_m \cos\theta \tag{3}$$

where γ_m is the lipid monolayer tension at the oil/water interface, as determined via pendant drop goniometry, and θ is the contact angle measured between the plane of the bilayer and the monolayer tangent line. The measured contact angles are reported in Figure S9. Negligible differences in monolayer tensions were observed between DOPC + NPs (γ_m = 0.37 ± 0.02 mN/m) and DOPC (γ_m = 0.37 ± 0.01 mN/m) and DPhPC + NPs (γ_m = 1.32 ± 0.01 mN/m) and DPhPC (γ_m = 1.29 ± 0.01 mN/m) in C10, n = 3 for all trials. The resulting bilayer tensions were calculated from these average monolayer tension values using eq 3 and are shown in Figure 5. The mean zero-volt γ_{app} values ranged from 0.7 to 2.5 mN/m, which are consistent with other DIB tensions[44] and about an order of magnitude higher than physiological membrane values.[60] For DPhPC + NP bilayers, γ_{app} was consistently higher than that for control DPhPC membranes at identical voltages (Figure 5A). This could be caused by the exposure of hydrophobic groups to the aqueous phase, which originates from the localized curvature around entrapped NPs.[29] For DOPC + NP bilayers, the tension followed previously observed non-monotonic trends; that is, γ_{app} increased at voltages approaching V_{crit} before decreasing after this point. For both lipid types, bilayer tension was higher when NPs were trapped in the membrane, signifying energetic penalties on lipid packing.

To quantify these changes, we calculated the energy of adhesion, ΔF[44]

$$\Delta F = 2\gamma_m(1 - \cos\theta) \tag{4}$$

which describes the reduction in free energy of the system upon bilayer formation. These values are shown in the insets of Figure 5 and were observed to increase gradually with voltage due to membrane thinning and area growth. ΔF was, on average, 0.0248 ± 0.0155 mJ/m^2 lower for DPhPC + NP membranes across all voltages when compared to the control case. This reduction confirmed that NPs were entrapped in DPhPC DIBs in C10 and incurred an energetic penalty on bilayer formation. Interestingly, ΔF for DOPC + NP membranes was initially similar to the control case and remained relatively constant at low voltages until V_{crit} was reached. Here, the mean value was at maximum 5.83 × 10^{-2} mJ/m^2 lower than the control condition. Thus, it appeared that entrapped NPs countered the effects of electrowetting and electrocompression, which otherwise increased adhesive energy in the control DOPC membrane. This remained true until the applied potential exceeded V_{crit}, upon which ΔF sharply increased. Still, the fact that values of ΔF remained lower in DOPC + NP bilayers even at high voltages shows that bilayer formation around NPs can be energetically unfavorable for both lipid types.

Upon application of a transmembrane potential, bilayer tension reduces by an amount $\Delta\gamma_{app}$. This occurs due to the increase of electrical energy at the interface and is balanced by a rise in disjoining pressure as the membrane thins. It is possible to calculate these electrical and mechanical contributions to tension and compare them to the measured values of $\Delta\gamma_{app}$. A difference in calculated and measured $\Delta\gamma_{app}$ implies that residual molecular interactions affect the bilayer tension, which can be grouped into a single term, $\Delta\gamma_{res}$.[47] The apparent membrane tension is thus calculated by

$$\Delta\gamma_{app} = \Delta\gamma_{EW} - \Delta\gamma_{strain} - \Delta\gamma_{res} \tag{5}$$

where the reduction of tension from electrical energy, which is responsible for electrowetting, is described by

$$\Delta\gamma_{EW} = \frac{1}{2}\frac{\varepsilon\varepsilon_0}{d_v}V^2 \tag{6}$$

and the strain contribution to tension, which arises from disjoining pressure and can be approximated by the Laplace pressure (P_{Lap}) and the pressure from the applied electric field (P_{Elec}), is described by

$$\Delta\gamma_{strain} = \int_{d_0}^{d_v} \left(\underbrace{\frac{\varepsilon\varepsilon_0}{2d^2}V^2}_{P_{Elec}} + \underbrace{\frac{2\gamma_m}{r}}_{P_{Lab}} \right) \mathrm{d}(d) \tag{7}$$

where d_v is the membrane thickness at a given voltage and r is the radii of the droplets, which are equal in volume and are assumed to remain constant under applied voltage.[47] Using eq 5 to compare calculated changes in apparent bilayer tension with those measured in Figure 5, it was observed that a positive value of $\Delta\gamma_{res}$ (mN m^{-1}) existed for both DOPC and DPhPC bilayers with and without NPs in C10, and that $\Delta\gamma_{res}$ increased monotonically with the variable strain energy term P_{Elec} (kPa). This implies the presence of an additional energetic penalty upon compression for all lipid conditions. These relationships

https://doi.org/10.1021/acsami.2c16677
ACS Appl. Mater. Interfaces 2022, 14, 54558−54571

may be approximated with linear models, depicted in Figure S10, which allows for comparison of sensitivities, as shown in Figure 6. The mean sensitivity of residual energy of DPhPC

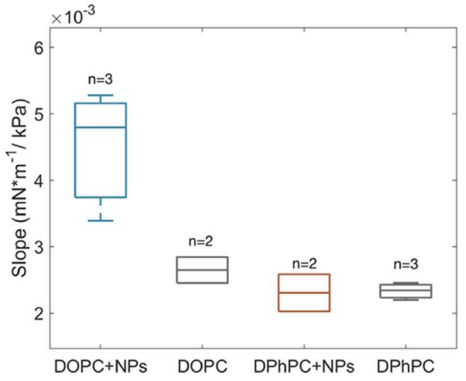

Figure 6. Sensitivity of changes in residual energy ($\Delta\gamma_{res}$, mN/m) to increasing compressive pressure (P_{Elec}, kPa) for bilayers with or without 0.1 mg/mL NPs. Test conditions and sample sizes are provided for each data set, and error bars represent one standard deviation.

membranes in C10 was 2.3 × 10^{-3} (mN m^{-1})/kPa, irrespective of whether NPs were present in the membrane. This value is the same order of magnitude as, but slightly higher than, the sensitivity of $\Delta\gamma_{res}$ for DPhPC lipids in C16 under applied voltage, which was previously attributed to the free lateral diffusion of lipids throughout the bilayer.[47] The value we report may be higher due to more rearrangement of oil in the membrane, as C10 molecules are squeezed out upon electrocompression. Similarly, DOPC membranes exhibited a mean sensitivity value of 2.6 × 10^{-3} (mN m^{-1})/kPa. However, the mean sensitivity for DOPC + NP membranes was 4.5 × 10^{-3} (mN m^{-1})/kPa, which is nearly twice as high as that for a NP-free membrane. This signified that when voltage increased the pressure across the membrane (and decreased its thickness), significant molecular rearrangement within the membrane occurred, establishing an energetic penalty that was evident from the difference in apparent and calculated bilayer tensions.

Lipid Structure Determines Embedded NP Distribution under Applied Potential. The incorporation of hydrophobic NPs into *n*-decane led to very different behaviors in DPhPC and DOPC bilayers, indicating the importance phospholipid tail structure on NP-membrane interactions. DPhPC exists in a fluid phase at room temperature,[61] though the methylated, saturated carbon tails impart enhanced stability and electrical resistance compared to other PC lipids.[62] Accordingly, DPhPC has a high bending modulus[63] (k_c = 12.8 ± 2.0 × 10^{-20} J) and does not easily accommodate NPs.[22] This likely causes a lower number of dispersed NPs to remain trapped in DPhPC bilayers upon DIB formation. Once embedded, NP aggregation is energetically favorable over dispersion within the membrane, since the clustering of hydrophobic inclusions reduces membrane bending energy.[22,24,59] However, an elastic energy barrier—which scales in magnitude with membrane bending rigidity[59]—exists between dispersed and aggregated NP distributions, which embedded NPs must first overcome before clustering. If this barrier exceeds energy from thermal fluctuations, membrane-mediated interactions will instead repel NPs from one another.[59]

Based upon the voltage-dependent properties of DPhPC + NPs, we believe that several aspects of our data can be explained by a homogeneous, dispersed NP distribution within the membrane across the entire tested voltage range, as depicted in Figure 7. Steric hindrance from dispersed NPs would lower adhesive energy between opposing monolayer leaflets and thereby dissociate planar DPhPC membranes at low transmembrane potentials. The identical sensitivities of $\Delta\gamma_{res}$ to compressive pressure for DPhPC and DPhPC + NP membranes also reveal no additional energetic penalty that would be expected for voltage-induced lateral diffusion of NPs. Further, while large or clustered NPs may increase the hydrophobic thickness of the bilayer, it was found elsewhere that hydrophobic NPs with 3 nm core diameters do not significantly change thickness of liposomal membranes,[19] as was observed here in DPhPC DIBs. Finally, the tendency to aggregate is reduced by residual alkane within the membrane, which fills energetically unfavorable void space between opposing lipid monolayers and hydrophobic NP inclusions.[20,24,53] On the nanoscale, embedded NPs have been shown to increase the area per lipid and membrane permeability in fluid phase bilayers,[19,26] which would enhance bilayer tension and conductivity as seen here. The NP presence in DPhPC is thus observed through the reduction in membrane-specific resistance, spontaneous leaflet dissociation (i.e., droplet separation) at low voltages, and increased bilayer tension, despite negligible differences in thickness. Hence, the presence of NPs could be missed via electrophysical measurements if only nominal values of capacitance were assessed.

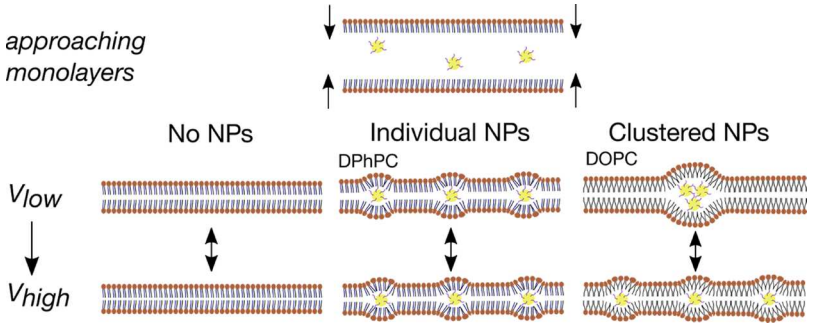

Figure 7. Approaching lipid monolayers trap NPs either as individually dispersed particles (e.g., in DPhPC) or clustered (e.g., in DOPC) distributions, depending on the bending rigidity of the lipid monolayers. Electrocompression squeezes out residual oil from the membrane interior, thinning the bilayer. If the NPs are clustered, pressure caused by a transmembrane potential can laterally disperse them, resulting in reversible, yet nonmonotonic, mechanical and electrical responses to applied voltage.

https://doi.org/10.1021/acsami.2c16677
ACS Appl. Mater. Interfaces 2022, 14, 54558−54571

DOPC membranes also exist in the fluid phase at room temperature,[64] though lipid disorder is enhanced by the presence of unsaturated bonds on the acyl chain tails.[61] Accordingly, the bending energy of DOPC is lower than DPhPC[63] (k_c = 11.0 × 10^{-20} J), which facilitates easier lateral diffusion of entrapped NPs. In other studies, lateral diffusion has been observed for embedded NPs in fluid phase lipid vesicles such as DOPC, but was negligible in more ordered membranes.[51] Further, MD simulations have revealed that low membrane tension reduces the free energy barrier between dispersed and aggregated states of embedded NPs.[65] We therefore propose that in contrast to DPhPC, the reduced bending stiffness and lateral tension of DOPC bilayers favors clustering of NPs within the DOPC DIB at low compressive pressures (i.e., low voltage), which then result in non-monotonic changes to *C* and *A* with increasing transmembrane potential. Aggregation explains why DOPC + NPs remain intact at 0 V: Consolidation of NP clusters enables the opposing monolayers to remain in contact with each other in regions devoid of NPs even in the absence of an external joining pressure. In addition, aggregates of small NPs are similar in size to NPs with larger diameters,[16] which can increase membrane thickness[19] as observed for DOPC + NP membranes at 0 V. Further, the average center-to-center distance calculated above for NPs in DOPC (6.7 nm) is on the same length scale as that required for aggregation of embedded NPs within a typical PC membrane.[59]

As voltage is applied to the DOPC + NP bilayer, electrocompressive forces act to disperse NP clusters; the apparent membrane tension rises, and the energy of adhesion decreases, as NPs are forced into energetically less favorable states. The lateral rearrangement of NPs in DOPC under compressive pressure is evidenced by the increased energetic penalty described in Figure 6. An increasing bias potential gradually reorganizes the phospholipids and NPs, and the corresponding tail disorder causes the DIB to thicken[64] as the membrane swells with oil. At a critical energy input V_{crit}, the dispersion of these clusters allows the membrane to thin until average thickness resembles that DOPC bilayers formed in the absence of NPs (Figure 7). In fact, this proposed high voltage state is mirrored in the similar thicknesses of DPhPC and DPhPC + NP membranes, which are assumed to retain individually dispersed NPs. When the entrapped NP concentration was increased, we observed a shift in V_{crit} to higher magnitudes. This implies that more energy was required to alter the initial particle distribution. In fact, as higher concentrations of NPs are trapped in the membrane, they become more likely to interact with each other at close distances;[59,65] this increases the number of aggregates, which requires a higher applied pressure to achieve a dispersed state. Finally, upon removal of applied voltage, the embedded NPs return to their energetically preferred state of aggregation within the fluid membrane. This reversible clustering is reminiscent of embedded NP behavior in membranes undergoing thermally driven phase transitions[55] and is facilitated by the steric repulsion of OT ligands bound to NPs.

In addition to NPs, it is important to consider the effects of residual alkanes trapped inside the membrane, which reside both parallel to and normal to the lipid tails.[43,66] Besides increasing the membrane thickness, alkanes can decouple opposing monolayers and reduce the bilayer bending modulus.[66] This likely increases the ability to trap hydrophobic molecules within the membrane. Trapped alkanes can also increase membrane surface defects,[67] though they only have marginal effects on the area per lipid and lateral lipid diffusion coefficients.[66,67] Both DPhPC and DOPC in C10 retain similar amounts of oil, as confirmed by comparable control thicknesses reported in Table S1 and accounting for longer DOPC tail length. This indicates that even though alkanes remain within the membrane, the lipid composition of the membrane still influences the behaviors of entrapped NPs. While the volumes of retained alkane herein are not biologically realistic, residual oil can be leveraged in future studies to replicate specific in vivo conditions; for example, apolar molecules such as squalene are produced by, and reside in, the center of the bilayer of the endoplasmic reticulum.[68] On the other hand, careful selection of NP core size and lipid bending moduli may enable particle entrapment in less oil-swollen membranes, such as those formed in C16. Further, application of transmembrane potential can greatly reduce the residual oil in the membrane, facilitating a more alkane-free environment.

CONCLUSIONS

In this paper, we explored the ability to trap hydrophobic NPs dissolved in oil between a DIB. We discovered that thinner membranes formed in *n*-hexadecane did not trap NPs, while thicker membranes formed in *n*-decane did. Entrapped NPs lowered membrane resistance, increased membrane tension, and reduced the energy of membrane adhesion. The more-rigid, liquid-ordered DPhPC bilayers did not easily bend to accommodate NP inclusions and required the application of DC voltage to remain intact; average thickness was not significantly different, suggesting that a low number of small NPs were embedded uniformly throughout the membrane and demonstrating that capacitance measurements used for thickness estimates alone may miss the presence of embedded NPs. In contrast, fluid DOPC bilayers enveloped NPs without requiring a holding potential and were twice as thick as a pure DOPC membranes, suggesting spontaneous clustering of NPs embedded in the bilayer. The liquid-disordered DOPC lipids enabled unique behaviors of entrapped NPs under applied voltage, including non-monotonic changes in capacitance and area with increasing voltage. We discovered that under an applied transmembrane potential, the compressive pressure forced NPs to reorganize within the membrane, creating further disorder before they dispersed to enable the exclusion of oil. This behavior was reversible upon decreasing the voltage, showing that NPs remained in the membrane and were not permanently excluded.

The reproducible entrapment of hydrophobic NPs provides a means to research material interactions within the phospholipid membrane, which retains clinical relevance for examining drug delivery and cytotoxicity. This can include in vivo scenarios where natural and engineered NPs are energetically driven into the hydrophobic membrane interior from the aqueous extracellular environment. Though the optical properties of gold NPs within membranes have been well studied, complementary electrical and mechanical probing of the membrane can reveal distinct properties, which are not apparent from physical aspects alone. The application of mechanical pressure through electrophysical analysis can also reveal structural alterations in the system due to field-induced pressure, such as the lipid-dependent NP-membrane interactions discussed here. These measurements are both fast and sensitive, so that time-resolved events like molecular insertion

https://doi.org/10.1021/acsami.2c16677
ACS Appl. Mater. Interfaces 2022, 14, 54558−54571

and pore formation could be studied in the future. Further incorporation of multiple lipid types[38] or transmembrane proteins[45,49] may also allow for detailed studies of specific biological systems. Other nanomaterials, especially voltage-sensitive particles such as quantum dots, may benefit from examination in this environment. Finally, the nontrivial effects of external voltage on trapped NPs may necessitate the application of this feature in future membrane models, as cells actively generate transmembrane potentials.

METHODS

Materials. OT-functionalized gold spherical NPs with a mean diameter of 3.28 ± 0.51 nm were purchased as powder from Nanoprobes, Inc. NPs were dissolved in toluene (Fisher Chemical) and stored at 2 °C until use. DPhPC and DOPC were purchased in chloroform from Avanti Polar Lipids. Both *n*-decane ($C_{10}H_{22}$) and *n*-hexadecane ($C_{16}H_{34}$) were purchased from Fisher Chemical at ≥98% purity. 10× PBS was purchased from Invitrogen and diluted to a 1x concentration (137 mM NaCl, 2.7 mM KCl, 8 mM Na2HPO4, and 2 mM KH2PO4) with Millipore Sigma Direct-Q deionized water (conductivity of 18.2 MΩ/cm) and then pH-adjusted with small amounts of hydrochloric acid to a physiological pH of 7.3.

Sample Preparation. To dissolve NPs within the oil phase, the NPs were placed under a gentle nitrogen stream and then put into a vacuum chamber until toluene was completely evaporated (≤6 h). Oil was used to solvate the NPs at a desired concentration, and the mixture was thoroughly shaken or vortexed until fully dissolved. Lipids in chloroform were similarly placed under a gentle nitrogen stream and then put into a vacuum chamber until chloroform was completely evaporated (≤3 h). The resultant lipid film was solvated with 1x PBS and vortexed until fully dissolved. The lipid solution was exposed to four freeze−thaw cycles and then extruded with Whatman track-etched polycarbonate 100 nm membranes to create monodisperse populations of unilamellar liposomes. Extruded lipid solutions were stored at 4 ° C until use. Ag/AgCl electrodes used in electrical measurements were prepared by soaking ball-tipped silver wire (Goodfellow) in bleach, rinsing, and then dipping the wire in molten agarose (Fisher BioReagents) to form a hydrophilic gel tip.

DLS and TEM. The solvated diameters of NPs in oil were measured using a Zetasizer Nano ZS DLS machine (ZEN3500, Malvern). Samples were loaded in a glass cuvette and illuminated with a laser, and the changing intensity in backscattered light was used to calculate particle size. For TEM measurements, OT NPs in toluene were combined with a dry DOPC film and mixed to homogenize the sample, before the toluene was evaporated in a vacuum chamber. The sample was then hydrated with deionized water and vortexed immediately for 5 min to introduce NPs to the assembling vesicle membranes. The sample then was stained with Uranyless and spread on a carbon-coated copper grid. Images were acquired using a Zeiss Libra 200 FE transmission electron microscope.

Broadband Dielectric Spectroscopy. Dielectric experiments were made using a Novocontrol High-Resolution Alpha Dielectric Analyzer at room temperature over a 0.1−10^6 Hz frequency range. The samples were measured between 20 mm diameter gold-plated brass electrodes using parallel plate capacitor geometry. The data are typically given in terms of the complex permittivity or complex dielectric function, $\varepsilon^*(\omega) = \varepsilon'(\omega) - i\varepsilon''(\omega)$. This can be related to the complex conductivity function as $\sigma^*(\omega) = i\omega\varepsilon_0\varepsilon^*(\omega)$. This can also be separated into its real and imaginary parts, $\sigma^*(\omega) = \sigma'(\omega) + i\sigma''(\omega)$. The frequency-independent value of the dielectric constant or coefficient (ε_s) can be observed as a plateau in $\varepsilon'(\omega)$. The magnitude of the applied AC voltage over the frequency range was 1.0 V.

Droplet Interface Bilayers. Aqueous droplets (400 nL) of 1x PBS containing 2 mg/mL lipid vesicles were pipetted onto electrodes connected to three-axis micromanipulators and an Axopatch 200B patch clamp amplifier, which supplied DC voltage. A low magnitude AC voltage (100 Hz, 10 mV triangle waveform) supplied using an external waveform generator (Agilent) was applied to measure capacitive current, i_c ($i_c = C\ dV/dt$). The picoamp current output was collected with a Digidata 1440 data acquisition system (Molecular Devices), and all measurements were made with appropriate shielding to reduce background noise to <±5 pA. In addition, extraneous pipette capacitance was minimized prior to each recording using Axopatch hardware. The pipetted droplets were incubated in an oil bath within a glass substrate until sufficient lipid monolayers formed at the oil−water interfaces (<10 min) and then were brought into contact with the micromanipulators. The area of contact was measured by calculating the major and minor elliptical axes from a combination of bottom-view and side-view cameras, which were connected to Dell monitors for live viewing, unless otherwise stated. Bilayer formation was confirmed via an increase in area and capacitive (square-wave) current. For experiments with dissolved NPs, a small backlight was used to illuminate the glass substrate for side-view imaging, as the oil solution was very dark. When necessary for formation, DC initiation voltages were increased in stepwise fashion for 1 minute at each value, until bilayer thinning was observed. All experiments were performed at room temperature (23 ° C). All quasi-static measurements were recorded only after steady-state current was observed. Membrane capacitance and resistance were extracted from current recordings using a custom Matlab script. Contact angles for bilayer tension measurements were likewise computed from bottom-view images using Matlab. For calculations of specific capacitance, we used the permittivity of carbon ($\varepsilon = 2.2$) because while functionalized gold NPs affect membrane permittivity,[31] dielectric measurements (Figure S2A) show that this effect is small (~6%) at 100 Hz, the frequency where C is assessed from measured current. Further, it is assumed that the permittivity is dominated by the hydrophobic lipid tail groups.

Pendant Drop. Pendant drop measurements for monolayer tension were made using a DataPhysics OCA 15EC device. Aqueous solutions were suspended vertically in a 250 μL Hamilton syringe with a Teflon-coated tip (0.73 mm outer diameter) and then dispensed slowly into a glass cuvette containing the oil phase for final droplet volumes of 0.5 μL (DPhPC) or 0.1 μL (DOPC). The shape of the pendant drop elongated with time as surfactant lipids adsorbed to the interface, which was captured with an integrated camera. The interfacial tension was calculated using a Laplace−Young fitting of the droplet profile with DataPhysics SCA20 software. Experiments were performed at room temperature, and all measurements were recorded until droplet equilibrium tension was reached.

ASSOCIATED CONTENT

Supporting Information

The Supporting Information is available free of charge at https://pubs.acs.org/doi/10.1021/acsami.2c16677.

Chemical structures, characterization of the nanoparticle/oil solutions, and various electrophysical measurements of embedded nanoparticles in bilayer structures (PDF)

AUTHOR INFORMATION

Corresponding Author

Stephen A. Sarles − *Mechanical Aerospace and Biomedical Engineering, University of Tennessee, Knoxville, Tennessee 37996, United States;* orcid.org/0000-0002-6694-6451; Email: ssarles@utk.edu

Authors

Colin M. Basham − *Mechanical Aerospace and Biomedical Engineering, University of Tennessee, Knoxville, Tennessee 37996, United States;* orcid.org/0000-0002-4364-221X

Stephanie Spittle − *Department of Chemical and Biomolecular Engineering, University of Tennessee, Knoxville, Tennessee 37996, United States*

Joshua Sangoro − *Department of Chemical and Biomolecular Engineering, University of Tennessee, Knoxville, Tennessee 37996, United States;* orcid.org/0000-0002-5483-9528

Joyce El-Beyrouthy − *School of Environmental, Civil, Agricultural, and Mechanical Engineering, University of Georgia, Athens, Georgia 30602, United States;* orcid.org/0000-0002-8038-4408

Eric Freeman − *School of Environmental, Civil, Agricultural, and Mechanical Engineering, University of Georgia, Athens, Georgia 30602, United States;* orcid.org/0000-0003-1209-9813

Complete contact information is available at: https://pubs.acs.org/10.1021/acsami.2c16677

Author Contributions

C.M.B. and S.A.S. designed and executed DIB measurements. C.M.B., S.S., and J.S. designed and executed impedance spectroscopy measurements and related analyses. C.M.B., S.A.S., J.E.-B., and E.F. executed the analysis of apparent membrane tension and developed the proposed mechanisms for NP organization in the membrane. All authors contributed to the manuscript preparation and have given approval to the final version of the manuscript.

Notes

The authors declare no competing financial interest.

■ ACKNOWLEDGMENTS

Transmission electron microscopy images were collected with support from the Advanced Microscopy and Imaging Center at the University of Tennessee, Knoxville. C.M.B. and S.A.S. acknowledge financial support from the National Science Foundation through CAREER Grant CBET-1752197. S.A.S. acknowledges financial support from the James Conklin Faculty Fellowship at the University of Tennessee, Knoxville. S.S. and J.S. acknowledge financial support from Breakthrough Electrolytes for Energy Storage (BEES), an Energy Frontier Research Center funded by the U.S. Department of Energy, Office of Science, Basic Energy Sciences under Award #: DE-SC0019409. J.E.-B. and E.F. graciously acknowledge support by NSF under grant #1903965.

■ REFERENCES

(1) Contini, C.; Schneemilch, M.; Gaisford, S.; Quirke, N. Nanoparticle−Membrane Interactions. *J. Exp. Nanosci.* **2018**, *13*, 62−81.

(2) Wu, G.; Mikhailovsky, A.; Khant, H. A.; Fu, C.; Chiu, W.; Zasadzinski, J. A. Remotely Triggered Liposome Release by near-Infrared Light Absorption Via Hollow Gold Nanoshells. *J. Am. Chem. Soc.* **2008**, *130*, 8175−8177.

(3) Amstad, E.; Kohlbrecher, J.; Müller, E.; Schweizer, T.; Textor, M.; Reimhult, E. Triggered Release from Liposomes through Magnetic Actuation of Iron Oxide Nanoparticle Containing Membranes. *Nano Lett.* **2011**, *11*, 1664−1670.

(4) Chen, Y.; Bose, A.; Bothun, G. D. Controlled Release from Bilayer-Decorated Magnetoliposomes Via Electromagnetic Heating. *ACS Nano* **2010**, *4*, 3215−3221.

(5) Zhou, X.; Moran-Mirabal, J. M.; Craighead, H. G.; McEUEN, P. L. Supported Lipid Bilayer/Carbon Nanotube Hybrids. *Nat. Nanotechnol.* **2007**, *2*, 185−190.

(6) Tunuguntla, R. H.; Escalada, A.; Frolov, V. A.; Noy, A. Synthesis, Lipid Membrane Incorporation, and Ion Permeability Testing of Carbon Nanotube Porins. *Nat. Protoc.* **2016**, *11*, 2029−2047.

(7) Liu, L.; Yang, C.; Zhao, K.; Li, J.; Wu, H.-C. Ultrashort Single-Walled Carbon Nanotubes in a Lipid Bilayer as a New Nanopore Sensor. *Nat. Commun.* **2013**, *4*, 2989.

(8) Saveleva, M. S.; Eftekhari, K.; Abalymov, A.; Douglas, T. E.; Volodkin, D.; Parakhonskiy, B. V.; Skirtach, A. G. Hierarchy of Hybrid Materials—the Place of Inorganics-in-Organics in It, Their Composition and Applications. *Front. Chem.* **2019**, *7*, 179.

(9) Sakaguchi, N.; Kimura, Y.; Hirano-Iwata, A.; Ogino, T. Fabrication of Au-Nanoparticle-Embedded Lipid Bilayer Membranes Supported on Solid Substrates. *J. Phys. Chem. B* **2017**, *121*, 4474−4481.

(10) Lee, H.-Y.; Shin, S. H. R.; Abezgauz, L. L.; Lewis, S. A.; Chirsan, A. M.; Danino, D. D.; Bishop, K. J. Integration of Gold Nanoparticles into Bilayer Structures Via Adaptive Surface Chemistry. *J. Am. Chem. Soc.* **2013**, *135*, 5950−5953.

(11) Michalet, X.; Pinaud, F. F.; Bentolila, L. A.; Tsay, J. M.; Doose, S.; Li, J. J.; Sundaresan, G.; Wu, A.; Gambhir, S.; Weiss, S. Quantum Dots for Live Cells, in Vivo Imaging, and Diagnostics. *Science* **2005**, *307*, 538−544.

(12) Al-Jamal, W. T.; Kostarelos, K. Liposomes: From a Clinically Established Drug Delivery System to a Nanoparticle Platform for Theranostic Nanomedicine. *Acc. Chem. Res.* **2011**, *44*, 1094−1104.

(13) Cormode, D. P.; Naha, P. C.; Fayad, Z. A. Nanoparticle Contrast Agents for Computed Tomography: A Focus on Micelles. *Contrast Media Mol. Imaging* **2014**, *9*, 37−52.

(14) Marshall, J. D.; Schnitzer, M. J. Optical Strategies for Sensing Neuronal Voltage Using Quantum Dots and Other Semiconductor Nanocrystals. *ACS Nano* **2013**, *7*, 4601−4609.

(15) Porret, E.; Sancey, L.; Martín-Serrano, A.; Montañez, M. I.; Seeman, R.; Yahia-Ammar, A.; Okuno, H.; Gomez, F.; Ariza, A.; Hildebrandt, N.; Fleury, J. B.; Coll, J. L.; le Guével, X. Hydrophobicity of Gold Nanoclusters Influences Their Interactions with Biological Barriers. *Chem. Mater.* **2017**, *29*, 7497−7506.

(16) Guo, Y.; Terazzi, E.; Seemann, R.; Fleury, J. B.; Baulin, V. A. Direct Proof of Spontaneous Translocation of Lipid-Covered Hydrophobic Nanoparticles through a Phospholipid Bilayer. *Sci. Adv.* **2016**, *2*, No. e1600261.

(17) Li, Y.; Chen, X.; Gu, N. Computational Investigation of Interaction between Nanoparticles and Membranes: Hydrophobic/Hydrophilic Effect. *J. Phys. Chem. B* **2008**, *112*, 16647−16653.

(18) Singh, P.; Pandit, S.; Mokkapati, V.; Garg, A.; Ravikumar, V.; Mijakovic, I. Gold Nanoparticles in Diagnostics and Therapeutics for Human Cancer. *Int. J. Mol. Sci.* **2018**, *19*, 1979.

(19) Chakraborty, S.; Abbasi, A.; Bothun, G. D.; Nagao, M.; Kitchens, C. L. Phospholipid Bilayer Softening Due to Hydrophobic Gold Nanoparticle Inclusions. *Langmuir* **2018**, *34*, 13416−13425.

(20) Nagao, M.; Bradbury, R.; Ansar, S. M.; Kitchens, C. L. Effect of Gold Nanoparticle Incorporation into Oil-Swollen Surfactant Lamellar Membranes. *Struct. Dyn.* **2020**, *7*, No. 065102.

(21) Prates Ramalho, J.; Gkeka, P.; Sarkisov, L. Structure and Phase Transformations of Dppc Lipid Bilayers in the Presence of Nanoparticles: Insights from Coarse-Grained Molecular Dynamics Simulations. *Langmuir* **2011**, *27*, 3723−3730.

(22) Perrotton, J.; Ahijado-Guzmán, R.; Moleiro, L. H.; Tinao, B.; Guerrero-Martinez, A.; Amstad, E.; Monroy, F.; Arriaga, L. R. Microfluidic Fabrication of Vesicles with Hybrid Lipid/Nanoparticle Bilayer Membranes. *Soft Matter* **2019**, *15*, 1388−1395.

(23) Preiss, M. R.; Hart, A.; Kitchens, C.; Bothun, G. D. Hydrophobic Nanoparticles Modify the Thermal Release Behavior of Liposomes. *J. Phys. Chem. B* **2017**, *121*, 5040−5047.

(24) Rasch, M. R.; Rossinyol, E.; Hueso, J. L.; Goodfellow, B. W.; Arbiol, J.; Korgel, B. A. Hydrophobic Gold Nanoparticle Self-Assembly with Phosphatidylcholine Lipid: Membrane-Loaded and Janus Vesicles. *Nano Lett.* **2010**, *10*, 3733−3739.

(25) Bonnaud, C.; Monnier, C. A.; Demurtas, D.; Jud, C.; Vanhecke, D.; Montet, X.; Hovius, R.; Lattuada, M.; Rothen-Rutishauser, B.; Petri-Fink, A. Insertion of Nanoparticle Clusters into Vesicle Bilayers. *ACS Nano* **2014**, *8*, 3451−3460.

(26) Park, S.-H.; Oh, S.-G.; Mun, J.-Y.; Han, S.-S. Loading of Gold Nanoparticles inside the Dppc Bilayers of Liposome and Their Effects on Membrane Fluidities. *Colloids Surf., B* **2006**, *48*, 112−118.
(27) Rasch, M. R.; Yu, Y.; Bosoy, C.; Goodfellow, B. W.; Korgel, B. A. Chloroform-Enhanced Incorporation of Hydrophobic Gold Nanocrystals into Dioleoylphosphatidylcholine (Dopc) Vesicle Membranes. *Langmuir* **2012**, *28*, 12971−12981.
(28) Wlodek, M.; Slastanova, A.; Fox, L. J.; Taylor, N.; Bikondoa, O.; Szuwarzynski, M.; Kolasinska-Sojka, M.; Warszynski, P.; Briscoe, W. H. Structural Evolution of Supported Lipid Bilayers Intercalated with Quantum Dots. *J. Colloid Interface Sci.* **2020**, *562*, 409−417.
(29) Chan, H.; Král, P. Nanoparticles Self-Assembly within Lipid Bilayers. *ACS Omega* **2018**, *3*, 10631−10637.
(30) Šegota, S.; Vojta, D.; Kendziora, D.; Ahmed, I.; Fruk, L.; Baranović, G. Ligand-Dependent Nanoparticle Clustering within Lipid Membranes Induced by Surrounding Medium. *J. Phys. Chem. B* **2015**, *119*, 5208−5219.
(31) Broda, J.; Setzler, J.; Leifert, A.; Steitz, J.; Benz, R.; Simon, U.; Wenzel, W. Ligand-Lipid and Ligand-Core Affinity Control the Interaction of Gold Nanoparticles with Artificial Lipid Bilayers and Cell Membranes. *Nanomed.: Nanotechnol., Biol. Med.* **2016**, *12*, 1409−1419.
(32) McCaig, C. D.; Song, B.; Rajnicek, A. M. Electrical Dimensions in Cell Science. *J. Cell Sci.* **2009**, *122*, 4267−4276.
(33) Levin, M. Molecular Bioelectricity in Developmental Biology: New Tools and Recent Discoveries: Control of Cell Behavior and Pattern Formation by Transmembrane Potential Gradients. *BioEssays* **2012**, *34*, 205−217.
(34) Mates, S. M.; Eisenberg, E. S.; Mandel, L. J.; Patel, L.; Kaback, H. R.; Miller, M. H. Membrane Potential and Gentamicin Uptake in Staphylococcus Aureus. *Proc. Natl. Acad. Sci. U. S. A.* **1982**, *79*, 6693−6697.
(35) Sahl, H.-G.; Kordel, M.; Benz, R. Voltage-Dependent Depolarization of Bacterial Membranes and Artificial Lipid Bilayers by the Peptide Antibiotic Nisin. *Arch. Microbiol.* **1987**, *149*, 120−124.
(36) Fleury, J.-B. Enhanced Water Permeability across a Physiological Droplet Interface Bilayer Doped with Fullerenes. *RSC Adv.* **2020**, *10*, 19686−19692.
(37) Basham, C. M.; Premadasa, U. I.; Ma, Y.-Z.; Stellacci, F.; Doughty, B.; Sarles, S. A. Nanoparticle-Induced Disorder at Complex Liquid−Liquid Interfaces: Effects of Curvature and Compositional Synergy on Functional Surfaces. *ACS Nano* **2021**, *15*, 14285−14294.
(38) Taylor, G. J.; Sarles, S. A. Heating-Enabled Formation of Droplet Interface Bilayers Using Escherichia Coli Total Lipid Extract. *Langmuir* **2015**, *31*, 325−337.
(39) Abdelhalim, M. A. K.; Mady, M. M.; Ghannam, M. M. Rheological and Dielectric Properties of Different Gold Nanoparticle Sizes. *Lipids Health Dis.* **2011**, *10*, 208.
(40) Venkatesan, G. A.; Taylor, G. J.; Basham, C. M.; Brady, N. G.; Collier, C. P.; Sarles, S. A. Evaporation-Induced Monolayer Compression Improves Droplet Interface Bilayer Formation Using Unsaturated Lipids. *Biomicrofluidics* **2018**, *12*, No. 024101.
(41) El-Beyrouthy, J.; Freeman, E. Characterizing the Structure and Interactions of Model Lipid Membranes Using Electrophysiology. *Membranes* **2021**, *11*, 319.
(42) Poulin, P.; Bibette, J. Adhesion of Water Droplets in Organic Solvent. *Langmuir* **1998**, *14*, 6341−6343.
(43) McIntosh, T.; Simon, S.; MacDonald, R. The Organization of N-Alkanes in Lipid Bilayers. *Biochim. Biophys. Acta Biomembr.* **1980**, *597*, 445−463.
(44) Taylor, G. J.; Venkatesan, G. A.; Collier, C. P.; Sarles, S. A. Direct in Situ Measurement of Specific Capacitance, Monolayer Tension, and Bilayer Tension in a Droplet Interface Bilayer. *Soft Matter* **2015**, *11*, 7592−7605.
(45) Bayley, H.; Cronin, B.; Heron, A.; Holden, M. A.; Hwang, W. L.; Syeda, R.; Thompson, J.; Wallace, M. Droplet Interface Bilayers. *Mol. BioSyst.* **2008**, *4*, 1191−1208.
(46) De Feijter, J.; Rijnbout, J.; Vrij, A. Contact Angles in Thin Liquid Films. I. Thermodynamic Description. *J. Colloid Interface Sci.* **1978**, *64*, 258−268.
(47) El-Beyrouthy, J.; Makhoul-Mansour, M. M.; Taylor, G.; Sarles, S. A.; Freeman, E. C. A New Approach for Investigating the Response of Lipid Membranes to Electrocompression by Coupling Droplet Mechanics and Membrane Biophysics. *J. R. Soc. Interface* **2019**, *16*, No. 20190652.
(48) Toma, H. E.; Zamarion, V. M.; Toma, S. H.; Araki, K. The Coordination Chemistry at Gold Nanoparticles. *J. Braz. Chem. Soc.* **2010**, *21*, 1158−1176.
(49) Koner, S.; Najem, J. S.; Hasan, M. S.; Sarles, S. A. Memristive Plasticity in Artificial Electrical Synapses Via Geometrically Reconfigurable, Gramicidin-Doped Biomembranes. *Nanoscale* **2019**, *11*, 18640−18652.
(50) Gross, L. C.; Heron, A. J.; Baca, S. C.; Wallace, M. I. Determining Membrane Capacitance by Dynamic Control of Droplet Interface Bilayer Area. *Langmuir* **2011**, *27*, 14335−14342.
(51) Gopalakrishnan, G.; Danelon, C.; Izewska, P.; Prummer, M.; Bolinger, P. Y.; Geissbühler, I.; Demurtas, D.; Dubochet, J.; Vogel, H. Multifunctional Lipid/Quantum Dot Hybrid Nanocontainers for Controlled Targeting of Live Cells. *Angew. Chem. Int. Ed.* **2006**, *118*, 5604−5609.
(52) Lin, X.; Gu, N. Surface Properties of Encapsulating Hydrophobic Nanoparticles Regulate the Main Phase Transition Temperature of Lipid Bilayers: A Simulation Study. *Nano Res.* **2014**, *7*, 1195−1204.
(53) Wi, H. S.; Lee, K.; Pak, H. K. Interfacial Energy Consideration in the Organization of a Quantum Dot−Lipid Mixed System. *J. Phys.: Condens. Matter* **2008**, *20*, No. 494211.
(54) Kalmbach, R.; Chizhov, I.; Schumacher, M. C.; Friedrich, T.; Bamberg, E.; Engelhard, M. Functional Cell-Free Synthesis of a Seven Helix Membrane Protein: In Situ Insertion of Bacteriorhodopsin into Liposomes. *J. Mol. Biol.* **2007**, *371*, 639−648.
(55) Von White, G.; Chen, Y.; Roder-Hanna, J.; Bothun, G. D.; Kitchens, C. L. Structural and Thermal Analysis of Lipid Vesicles Encapsulating Hydrophobic Gold Nanoparticles. *ACS Nano* **2012**, *6*, 4678−4685.
(56) Su, C.-F.; Merlitz, H.; Rabbel, H.; Sommer, J.-U. Nanoparticles of Various Degrees of Hydrophobicity Interacting with Lipid Membranes. *J. Phys. Chem. Lett.* **2017**, *8*, 4069−4076.
(57) Taylor, G.; Nguyen, M.-A.; Koner, S.; Freeman, E.; Collier, C. P.; Sarles, S. A. Electrophysiological Interrogation of Asymmetric Droplet Interface Bilayers Reveals Surface-Bound Alamethicin Induces Lipid Flip-Flop. *Biochim. Biophys. Acta Biomembr.* **2019**, *1861*, 335−343.
(58) Nakamura, H.; Sezawa, K.; Hata, M.; Ohsaki, S.; Watano, S. Direct Translocation of Nanoparticles across a Model Cell Membrane by Nanoparticle-Induced Local Enhancement of Membrane Potential. *Phys. Chem. Chem. Phys.* **2019**, *21*, 18830−18838.
(59) Daniel, M.; Řezníčková, J.; Handl, M.; Iglič, A.; Kralj-Iglič, V. Clustering and Separation of Hydrophobic Nanoparticles in Lipid Bilayer Explained by Membrane Mechanics. *Sci. Rep.* **2018**, *8*, 10810.
(60) Garten, M.; Mosgaard, L. D.; Bornschlögl, T.; Dieudonné, S.; Bassereau, P.; Toombes, G. E. Whole-Guv Patch-Clamping. *Proc. Natl. Acad. Sci. U. S. A.* **2017**, *114*, 328−333.
(61) Kučerka, N.; Nieh, M.-P.; Katsaras, J. Fluid Phase Lipid Areas and Bilayer Thicknesses of Commonly Used Phosphatidylcholines as a Function of Temperature. *Biochim. Biophys. Acta Biomembr.* **2011**, *1808*, 2761−2771.
(62) Velikonja, A.; Kramar, P.; Miklavčič, D.; Lebar, A. M. Specific Electrical Capacitance and Voltage Breakdown as a Function of Temperature for Different Planar Lipid Bilayers. *Bioelectrochemistry* **2016**, *112*, 132−137.
(63) Chaurasia, A. K.; Rukangu, A. M.; Philen, M. K.; Seidel, G. D.; Freeman, E. C. Evaluation of Bending Modulus of Lipid Bilayers Using Undulation and Orientation Analysis. *Phys. Rev. E* **2018**, *97*, No. 032421.

https://doi.org/10.1021/acsami.2c16677
ACS Appl. Mater. Interfaces 2022, 14, 54558−54571

(64) Taylor, G. J.; Heberle, F. A.; Seinfeld, J. S.; Katsaras, J.; Collier, C. P.; Sarles, S. A. Capacitive Detection of Low-Enthalpy, Higher-Order Phase Transitions in Synthetic and Natural Composition Lipid Membranes. *Langmuir* **2017**, *33*, 10016−10026.
(65) Tian, F.; Zhang, X.; Dong, W. How Hydrophobic Nanoparticles Aggregate in the Interior of Membranes: A Computer Simulation. *Phys. Rev. E* **2014**, *90*, No. 052701.
(66) Usuda, H.; Hishida, M.; Kelley, E. G.; Yamamura, Y.; Nagao, M.; Saito, K. Interleaflet Coupling of N-Alkane Incorporated Bilayers. *Phys. Chem. Chem. Phys.* **2020**, *22*, 5418−5426.
(67) Zoni, V.; Campomanes, P.; Vanni, S. Investigating the Structural Properties of Hydrophobic Solvent-Rich Lipid Bilayers. *Soft Matter* **2021**, *17*, 5329−5335.
(68) Santinho, A.; Chorlay, A.; Foret, L.; Thiam, A. R. Fat Inclusions Strongly Alter Membrane Mechanics. *Biophys. J.* **2021**, *120*, 607−617.

https://doi.org/10.1021/acsami.2c16677
ACS Appl. Mater. Interfaces 2022, 14, 54558−54571